ORIGINAL RESEARCH ARTICLE

Assessment of cerebral venous sinus: Anatomical and functional diagnostic performance of three-dimensional reconstruction models based on venous sinus MRI and CT images

Xin Liu[1†] , **Zhenxin Hong**[2†] , **Heyu Ding**[3†] , **Pengfei Zhao**[3] , **Shusheng Gong**[4] , **Dhanjoo Ghista**[5] , and **Zhenchang Wang**[3]*

[1]Guangdong Academy Research on VR Industry, School of Industrial Design and Ceramic Art, Foshan University, Foshan, Guangdong, China

[2]Department of Industrial Robotics, School of Artificial Intelligence, Guangdong Engineering Polytechnic College, Qingcheng, Guangdong, China

[3]Department of Radiology, Beijing Friendship Hospital, Capital Medical University, Beijing, China

[4]Department of Otolaryngology, Head and Neck Surgery, Beijing Friendship Hospital, Capital Medical University, Beijing, China

[5]University 2020 Foundation, San Jose, California, United States of America

Abstract

Venous sinus stenosis is commonly observed in patients presenting with pulsatile tinnitus (PT). While magnetic resonance imaging (MRI) and computed tomography (CT) are commonly used for assessing venous sinus geometries, the preferred modality remains unclear. In this study, we reconstructed the three-dimensional (3D) geometries of the venous sinus using MRI and CT imaging data from 20 PT patients. We conducted comparisons of the anatomical features of the venous sinus through case-wise analysis and anatomic geometrical parameter-wise analysis. Our findings indicate that by taking the geometries from CT as a reference, MRI could provide a better illustration of venous structure, primarily due to a stronger flow signal concentrated in the vascular tree. We observed high agreements in anatomic parameters measured from 3D geometries reconstructed based on CT and MRI in 19 out of 20 cases. Notably, the cross-sectional area of the sinus and segment length displayed the highest consistency, with a mean difference of -5.01% and 6.5% between modalities, respectively. In addition, we noticed that 55% of cases exhibited consistency in analyzing the confluence of the sinus, while variants of connectivity and collateral branching were observed between CT and MRI. Importantly, CT-based geometric reconstruction provided better detail of inflow side branches in the straight sinus, whereas MRI preserved more side branches of outflow in the downstream sinus. It is important to note that CT-based evaluation may be affected by the bone structures surrounding the venous sinus, whereas MRI-based evaluation focuses on blood flow to the segments, potentially indicating both anatomical and functional abnormalities.

Keywords: Cerebral venous sinus; Pulsatile tinnitus (PT); Magnetic resonance imaging (MRI); Computed tomography

1. Introduction

Pulsatile tinnitus (PT) is often related to an underlying vascular abnormality, significantly affecting the patient's quality of life.[1] Cerebral venous stenosis-induced PT has gained increasing recognition, with venous sinus stenting (VSS) emerging as an effective treatment option for symptom relief.[2] Transverse sinus stenosis (TSS) is a commonly observed vascular abnormality in patients with PT.[3] The previous studies have highlighted the high diagnostic performance of both computed tomography venography (CTV) and magnetic resonance venography for anatomical analysis of venous sinuses.[4] The choice of modality generally depends on availability, although comparisons between modalities have been rarely assessed.

Anatomical assessment is widely conducted using CTV and Phase-contrast magnetic resonance imaging (MRI).[5,6] Computed tomography (CT) remains the primary approach for differentiating the source of vascular-related tinnitus, due to its high spatial resolution and consequent high diagnostic accuracy.[3] On the other hand, MRI has increasingly been applied for intracranial venous assessment, offering advantages such as superior soft-tissue contrast without interference bone structures, as shown in CT images.[7-9] Therefore, MRI is considered a promising tool for analyzing the vasculature and the defects of surrounding tissues, including vascular interface, meningeal defects, and related malformations.[7,9] However, the previous studies have reported potential false-positive diagnoses due to slow blood flow and artifacts in MRI, leading to ongoing debates regarding abnormalities in unilateral transverse dural sinuses and transverse sinuses (TSs).[10,11]

This study aims to assess the anatomical parameters of the venous sinus based on MRI from patients with PT, with CTV as a reference. For this purpose, three-dimensional (3D) anatomies were reconstructed from medical images for quantitative and qualitative evaluations.

2. Methods

2.1. Datasets

Patients with PT were retrospectively selected from Beijing Friendship Hospital, Capital Medical University, between March 13, 2019, and August 26, 2019. Inclusion criteria consisted of undergoing CTV and MRI within 3 months of the CTV examination. Exclusion criteria included previous stenting and the presence of venous sinus thrombosis, neoplasms, or arterial/arteriovenous abnormalities. This study was approved by the Institutional Review Board, and informed consent was obtained from all patients. A total of 20 patients, aged between 23 and 60 years with a mean age of 42 ± 12 years, were included in the present study.

2.2. Image acquisitions

The MRI data were acquired using a 3.0T MRI unit (Ingenia, Philips Healthcare, Netherlands) equipped with a 16-channel head coil. The MRI examinations employed a 3D phase-contrast technique using a gradient-echo sequence with the following parameters: field of view of $173 \times 173 \times 192$ mm^3, repetition time of 17 ms, echo time of 6.2 ms, flip angle of 10°, velocity encoding of 15 cm/s, bandwidth of 230 Hz/pixel, matrix size of $144 \times 108 \times 120$, and acquisition time of 2 min 15 s.

CTV images were acquired using a 256-section CT scanner (Revolution, GE Healthcare, US) with the following parameters: tube voltage of 100 kV, 25 mAs (auto-mAs), matrix of 512×512, collimation of 256×0.625 mm, rotation time of 0.5 s, pitch of 0.992:1, and administration of contrast media (iopamidol, Bracco Diagnostics, UK) at a concentration of 370 mg iodine/ml, 1.5 ml/kg, injected at a rate of 5 ml/s. The average CT dose index (CTDI) was 63.95 mGy, and the average total dose length product (DLP) was 664.3 mGy·cm.

2.3. Reconstruction of 3D geometry models

The anatomies of the cases were reconstructed using Mimics 19.0 (Materialise, Belgium). The region of interest was segmented based on the signal intensity distribution of MRI and CTV images. Consultation with clinical technicians was conducted to improve the accuracy of 3D geometric reconstruction. The major segments of the intracranial venous network were evaluated, including the TSs, sigmoid sinuses (SSs), straight sinuses (StSs), inferior sinus, and superior sagittal sinuses (SSSs), as illustrated in Figure 1.
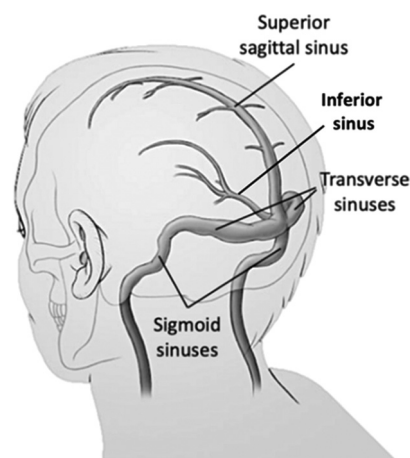

Figure 1. Intracranial venous network. The network encompasses superior sagittal sinus, transverse sinuses, sigmoid sinuses, and inferior sinuses.

2.4. Anatomical parameters for comparison

The anatomical parameters for comparison included the minimum and maximum cross-sectional area of the segment (CSA), degree of stenosis calculated as the ratio between the minimum and maximum CSA, volume (V) of the segment, segment length of the sinus (SL), the angle of the segment (α), and average curvature of the segment (Equation I):

$$\text{Curvature} = \left| \frac{\text{SL}}{\alpha} \right|$$

(I)

In addition, the length of the venous stenosis (Figure 2) was measured. The number of parameters ranged from 31 to 46, depending on the presence of the segments. Both sinus segment-wise and case-wise analyses were conducted. Intraobserver analysis was conducted to evaluate the consistency of anatomical parameter measurements. Repeated measurements were performed by the same reviewer within 1 week. The diameter ratio (DIAR) between CTV- and MRI-based measurements was used as an indicator for analysis. DIAR was calculated as follows (Equation II):

$$\text{DIAR} = \frac{\left(\text{CTV}_{\text{Diameter}} - \text{MRI}_{\text{Diameter}} \right)}{\text{CT}_{\text{Diameter}}}$$

(II)

In cases where a segment was absent, its diameter was represented as 0. Specifically, if a segment was absent in the CTV-based geometry, the denominator of DIAR was replaced by $\text{MRI}_{\text{Diameter}}$.

We conducted a sinus-wise analysis by comparing the number of entrances and exits of each sinus and major venous sinuses, including the SSS, inferior sinus, StS, TS, and SS. An agreement number was used to show the difference in collateral branches, which was defined as the ratio of cases with the same number of visible side branches in both CTV and MRI to the number of cases in CTV. A cross-reference analysis was conducted, and the number of missing entrances and exits was recorded.

In addition, we conducted a case-wise analysis of anatomical parameters based on MRI-reconstructed geometries by taking those from CTV-based geometries as references.

The development of the eye ring occurs during the four to 6 months of pregnancy, during which a series of primitive dura mater and dural sinus transitional growth and degeneration patterns occur. Irregular growth patterns can lead to asymmetry of the dural sinuses of varying heights and sizes, mild to obvious irregularities, and even loss of the inner TS.[12,13] The previous studies have illustrated six distinguished types of sinus confluence (connecting points) as follows: Type 1 indicates that the StSs are connected with the left and right TSs and the SSSs. Type 2a and 2b indicate that the StS is connected to the left or right TS. Type 3 is SSS and StS branching to bilateral TS. Types 4a and 4b indicate that the left or right TS is not connected. Types 5a and 5b indicate that an additional connecting vein is found between the StS and the SSS on both sides. Type 6 is the oblique sinus. These confluences are illustrated in Figure 3.[14] As the pattern of confluence sinus could be an important factor for evaluating the drainage of the blood flow in the sinus, a comparison of confluence classification using CTV and MRI was conducted.

2.5. Statistical analysis

Data analysis was performed using SPSS24.0 software (SPSS Inc., USA). Continuous variables, when appropriate, are expressed as mean±standard deviation (SD) or median (interquartile range [IQR]). Differences were assessed using the Bland-Altman test for consistency. Categorical variables are expressed as frequencies and percentages. Correlation analysis was conducted to examine the correlation between CTV and MRI anatomical structure parameters using correlation coefficients. $P < 0.01$ was considered statistically significant.
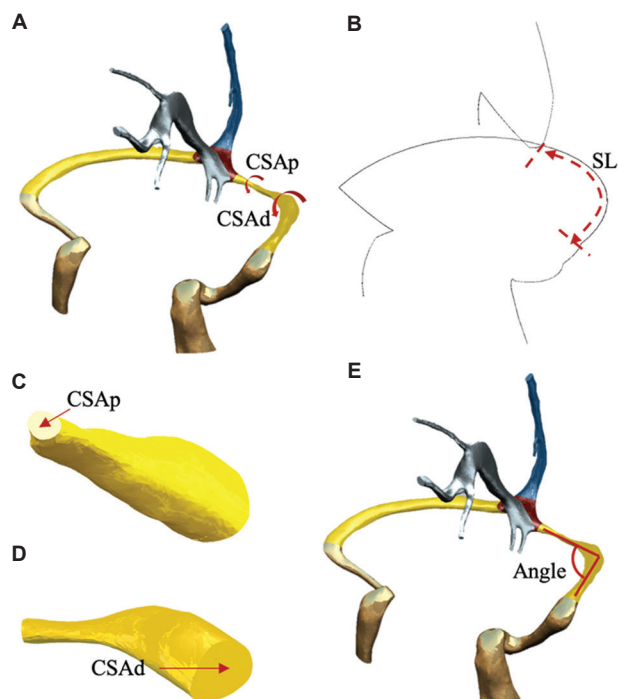

Figure 2. A schematic of the anatomical parameter extraction. This schematic illustrates the extraction of anatomical parameters from the 3D reconstructed geometry, specifically focusing on the segment of the transverse sinus. (A) The minimum and maximum cross-sectional areas of the segment are denoted as CSAp and CSAd, as shown in (C) and (D), respectively. (B) The measurement of segment length (SL). (E) The angle of the segment, with the recorded number of angles depending on the number of angles visible in the reconstructed geometry.
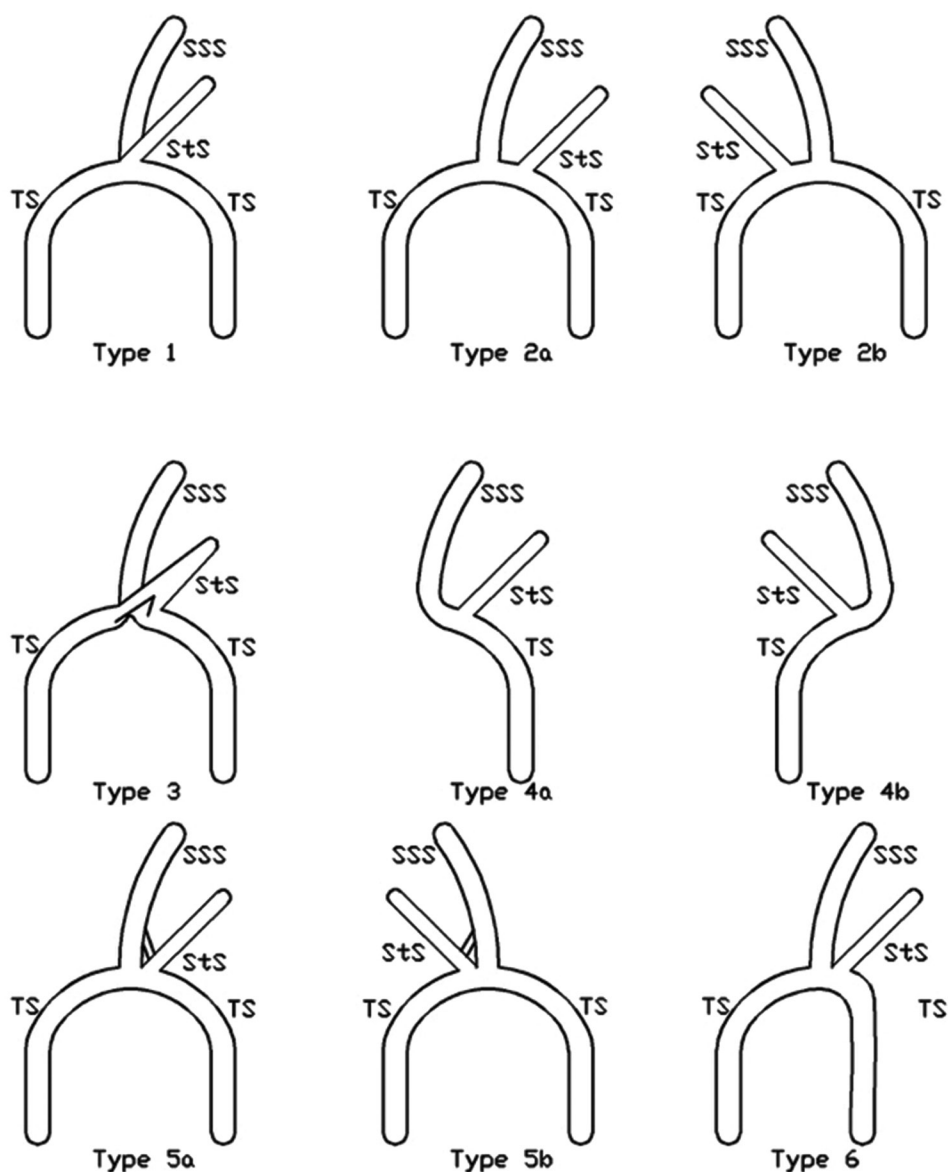
Figure 3. The schematics of six types of confluences
Abbreviations: SSS: Superior sagittal sinus; StS: Straight sinus; TS: Transverse sinus.

3. Results

In all cases, 3D geometries were successfully reconstructed from both CTV and MRI datasets. Figure 4 illustrates comparisons of segments reconstructed from CTV and MRI data. While the TS was identifiable in both CTV and MRI, the MRI images presented a stronger signal at the left TS (normalized against the surrounding structures) compared to those in the CTV images (A2 and B2). Segments are highlighted in colors. As an example, the comparisons of segments revealed a variation in visually available bifurcation at SSS between the geometric reconstructions based on MRI and CTV.

3.1. Comparison of anatomic parameters between CTV and MRI

In the sinus-wise analysis, a high degree of consistency (65%) was observed in SSS, with an average of one visible branch in both CTV and MRI. Compared to MRI, CTV exhibited more entrances to StS, with an agreement rate of 15%. The average number of visible branches in CTV and MRI was 6 and 5, respectively. On the other hand, MRI
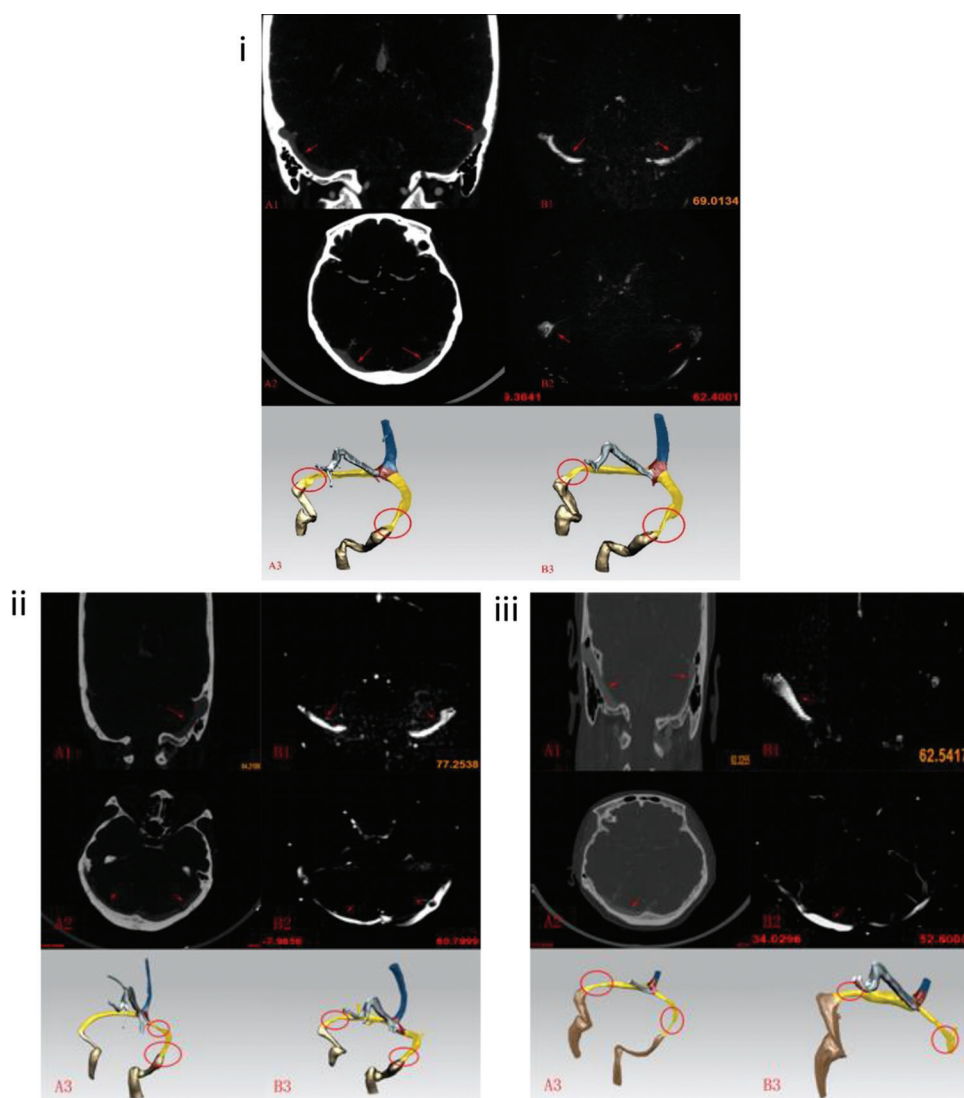
Figure 4. Comparison models of computed tomography venography (CTV) (images labeled by A) and magnetic resonance imaging (images labeled by B). A1 and B1 are coronal planes with transverse sinuses (indicated by red arrows); A2 and B2 are axial planes with transverse sinuses (indicated by red arrows); A3 and B3 are geometries reconstructed based on CTV and MRI images, respectively. Segments are highlighted in colors as follows: the superior sagittal sinus (blue), the left and right transverse sinuses (yellow), the left and right sigmoid sinuses (gold), the inferior sinus (silver), and the confluence of the segments (brown). Stenosis is highlighted with red circles. Panels i, ii, and iii represent Cases 3, 2, and 19, respectively.

demonstrated more TS outlets compared to CTV, with an agreement rate of 15% and an average of one and three visible branches in CTV and MRI, respectively. Similarly, MRI displayed more of the SS outlets compared to CTV, with an agreement rate of 25%. Detail distributions of inlets and outlets for CTV- and MRI-based geometric reconstructions are shown in Figure A1.

The case-wise analysis of anatomical parameters for each segment is illustrated in Figure 5. In general, the results demonstrated a robust correlation in ten out of 20 cases (correlation coefficient >0.9), a moderate correlation in nine out of 20 cases (correlation coefficient >0.5), and one case with a poor correlation (correlation coefficient = 0.28). Bland-Altman analysis indicated agreement between MRI- and CTV-based evaluations. Specifically, good consistency was observed in the CSA and segment lengths, while high variations were found in other parameters due to differences in visible-based reconstructions. Figure 6 illustrates the comparison of anatomical parameters in the best- and worst-correlated cases.

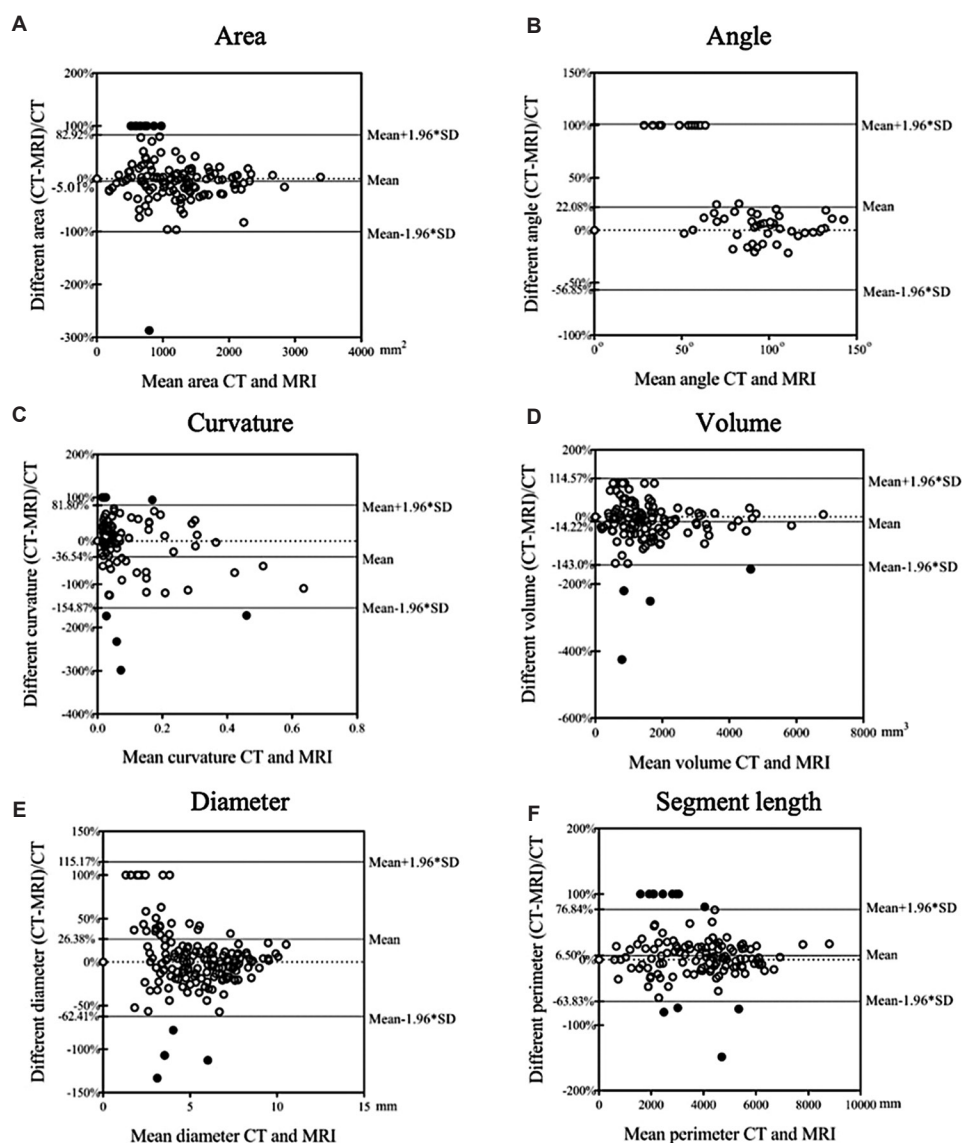The intraobserver analysis showed high consistency of the measurements from geometries reconstructed CTV

Figure 5. The case-wise analysis of anatomical parameters for each segment. This figure presents the geometrical parameters of all cases. (A) Cross-section area: Mean difference (−5.01%) and range of limits (82.92%, −100%). (B) Angle: Mean difference (22.08%) and range of limits (100%, −56.85%). (C) Curvature: Mean difference (−36.54%) and range of limits (81.80%, −154.87%). (D) Volume: Mean difference (−14.22%) and range of limits (114.57%, −143.0%). (E) Diameter: Mean difference (26.38%) and range of limits (115.17%, −62.41%). (F) Segment length: Mean difference (6.50%) and range of limits (76.84%, −63.83%). Abbreviations: CT: Computed tomography; MRI: Magnetic resonance imaging; SD: Standard deviation.

and MRI. Repeated measurements were 1 week after the first measurements. The reviewer was blinded to the recorded results and locations of measurement. The DIAR between CTV- and MRI-based measurements was taken as an indication for the analysis. The indicator segment-wise correlation analysis was conducted for all cases. The results of each venous sinus segment were recorded separately. The correlation analysis is shown in Figure 7, whereas the coefficients are shown in Table 1.

3.2. Comparison of the confluence of the sinus

The distribution of confluences in our dataset was determined using the CTV-based analysis as a reference. In general, the patterns of confluence analyzed using MRI images displayed agreement with CTV-based analysis in 55% of cases (11 out of 20). Comparisons between CTV and MRI are illustrated in Figure 8. The majority of the cases fall in the Type 2 category for both CTV- and MRI-
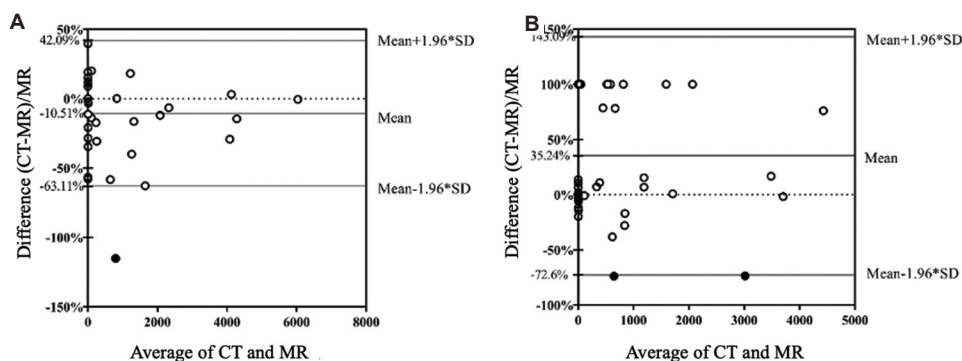
Figure 6. The comparison of anatomical parameters in the best- and worst-correlated cases. (A) The best-correlated case displays a Pearson coefficient value of 0.992, with a mean difference of 10.51% and a range of limits of (42.09%, −63.11%). (B) The worst-correlated case displays a Pearson coefficient value of 0.258, with a mean difference of 35.24% and a range of limits of (143.09%, −72.60%). Abbreviations: CT: Computed tomography; MRI: Magnetic resonance imaging; SD: Standard deviation.
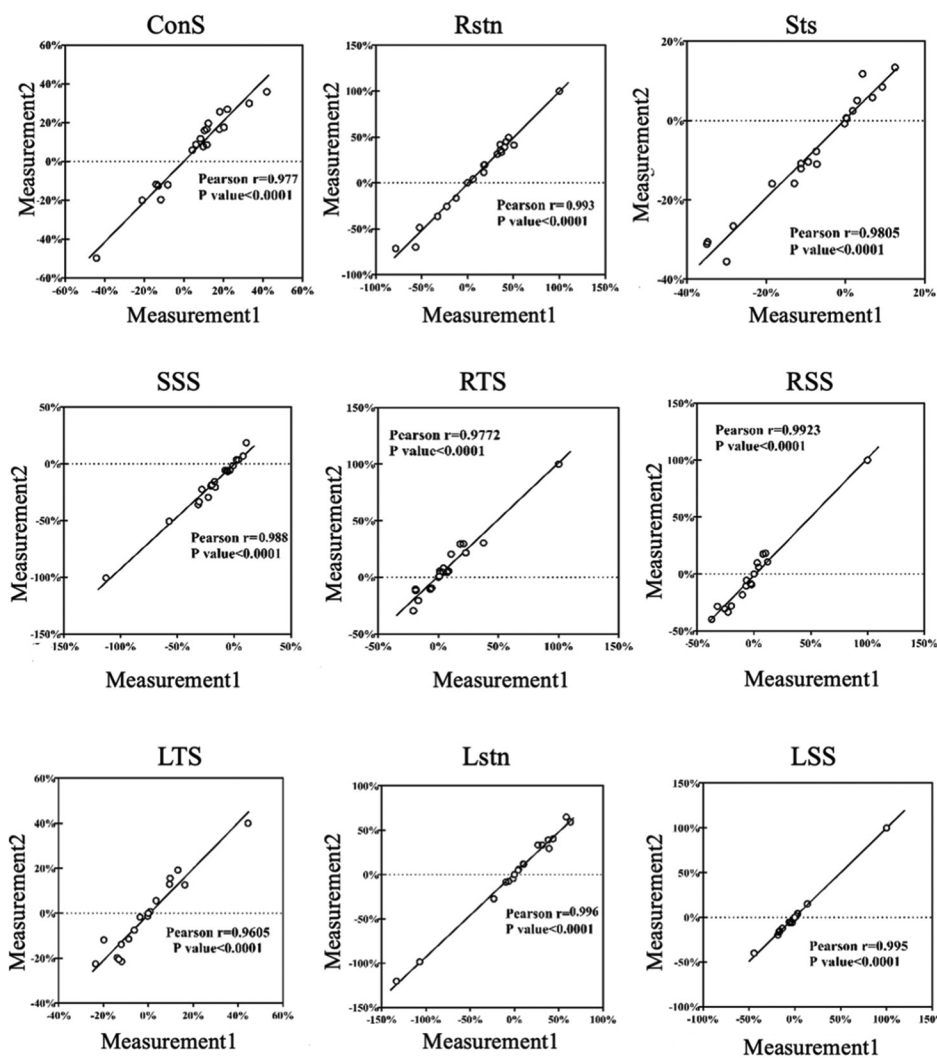
Figure 7. Intraobserver analysis using the differences in diameters between computed tomography venography (CTV) – and magnetic resonance imaging (MRI)-based measurements as indications. The correlation plots of repeating measurements for the following segments: Confluence sinus (ConS), right stenosis (Rstn), straight sinus (StS), superior sagittal sinus (SSS), right transverse sinus (RTS), right sigmoid sinus (RSS), left transverse sinus (LTS), left stenosis (Lstn), and left sigmoid sinus (LSS).

Table 1. Results of the repeated measurement for intraobserver analysis using diameter ratio as an indicator

Segments	ConS	Rstn	Sts	SSS	RTS	RSS	LTS	Lstn	LSS
Correlations	0.977	0.993	0.9805	0.988	0.9772	0.9923	0.9605	0.996	0.995

Abbreviations: ConS: Confluent sinus; LSS: Left sigmoid sinus; Lstn: Left stenosis; LTS: Left transverse sinus; RSS: Right sigmoid sinus; Rstn: Right stenosis; RTS: Right transverse sinus; SSS: Superior sagittal sinus; Sts: Straight sinus.

based analysis (20% and 35%, respectively). The number of cases for Type 4a and Type 6 was consistent between CTV and MRI (Two cases each for Type 4a and 1 case for Type 6). Variations in confluence were observed in other types (Figure 9). Specifically, the Type 3 confluence was identified based on CTV-based analysis in four cases (Cases 1, 7, 9, and 12, as illustrated in Figure A1), while in MRI-based analysis, these cases were identified as Types 4a, 2a, 2b, and 4a. Significant variations in confluence were observed in Cases 2, 11, and 17, where StS joined with the contralateral TS in MRI compared to CTV. Meanwhile, the small side branch originating from SSS was observed in CTV for Case 20, which was absent in MRI.

4. Discussion

A robust correlation and good agreement were evident in the sinus geometries when comparing the reconstructed geometries based on CTV and MRI. Sinus-wise analysis indicated that, with few exceptions observed in particular segments, MRI-based geometries preserved more side branches compared to CTV-based ones (Figure A1). However, despite these positive findings, several concerns remain regarding the use of MRI for the assessment of the venous sinus.

4.1. Classification of the confluence of the sinus

The previous studies have established the reliability of CT and MRI for vascular imaging. Nevertheless, both methods have limitations. The imaging of blood vessels in CT is affected by bone structures, contrast agents, and blood density,[15] while MRI is affected by the direction of blood flow, signal strength, and artifacts.[10] In addition, the confluence of the sinus is more discernible in CT due to the straightforward blood flow directions from SSS, StS, and TSs to the confluence sinus (Figure A2). Conversely, MRI may not clearly depict this confluence due to the complexity of blood flow directions. Notably, the density difference facilitates the recognition of the confluence sinus in CTV. Similarly, both modalities typically display a Type 1 confluence sinus in cases where the left and right TSs are connected (Figure 2), while Type 4 is observed in cases of unilateral TS and Type 6 in cases of an oblique sinus.[16] In addition, MRI may fail to capture the round Torcular Herophili type (Type 3) in all cases. Variations in geometric reconstruction arise from differences in the
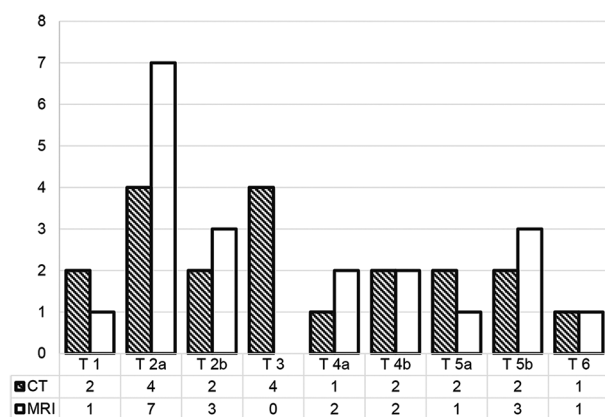

Figure 8. The distribution of the confluence variations. Type 1 to Type 6 indicated the nine types of confluence, as shown in **Figure 3**. Abbreviations: CT: Computed tomography; MRI: Magnetic resonance imaging; T: Type.

visibility of blood flow in images obtained from CTV and MRI (Figure 5). In particular, SS could be captured in CTV images but not in MRI images in certain cases (Figure A2), resulting in a 100% difference, as shown in Figure 4. Importantly, the volume of the geometries is significantly impacted by the absence of the sinus in MRI compared to CTV-based assessment.

Moreover, different patterns of confluent sinuses may introduce variability into the image-based assessment of the venous sinus system. Among these configurations, the circular torcular Herophili type exhibited higher overall accuracy when evaluated using CTV, a finding not significantly recognized by MRI. However, our results indicate that MRI is more adept at evaluating the dominant phenomenon of the TS, in line with previous reports.[13] Although this observation remained consistent in the segment-wise analysis of each venous sinus, other confluent sinus types exhibited a high disagreement rate (45%) when comparing MRI to CTV in our patient population with PT. In addition, Type 4b and Type 6 configurations could be misinterpreted as the same confluent sinus when using MRI. The misinterpretation of the absent TS may stem from challenges in detecting blood flow, which could be either hindered by variations in venous sinus anatomy or masked by surrounding bone structures.
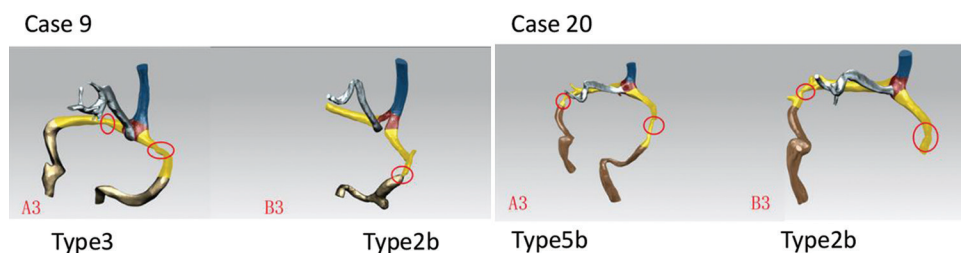
Figure 9. An illustration of the Variations in confluences of sinuses that are categorized into different types of patterns: Case 9. Type 3 and Type 2b; Case 20. Type 5b and Type 2b.

4.2. Side branch assessment

CTV and MRI have been used to assess venous sinus abnormalities for the diagnosis of PT, including stenosis, collateral sinus, and hypoplastic veins. However, Guryildirim *et al.* demonstrated that the accuracy of identifying blood vessels with a diameter less than 3 mm on CT images ranged 90 – 94%.[17] Conversely, accuracy reached 100% for blood vessels with a diameter exceeding 4 mm.[18] On the other hand, Gao *et al.* stated that MRI exhibited a specificity of over 94% and a sensitivity was 86% for detecting cerebral venous sinus thrombosis.[19] Our results revealed variability in the detection of small side branches between CTV and MRI. Notably, the SSS segment demonstrated the highest level of agreement in side branch detection when comparing MRI to CTV. In addition, MRI detected more side branches in the TS and SS. The signal flow indicated by MRI could enhance the contrast of the vascular tree against surrounding structures, potentially improving the identification of small branches compared to CTV. This enhancement might be attributed to the similar grayscale resolution of the contrast agent in small side branches compared to adjacent tissue.

In instances of complex cerebral venous sinus anatomy, collateral drainage vessels may transform into main venous outflow channels when positioned upright.[20-22] Mazur *et al.* have reported that if ligation of one TS within the venous sinus is necessary, the contralateral sinus must remain patent or exhibit sufficient drainage before surgery.[23] Similarly, Sheth *et al.* noted that a decreased number of collateral circulation vessels correlates with poorer outcomes in patients with dural venous sinus thrombosis.[24] Venous sinus occlusion can exacerbate brain swelling due to interrupted venous drainage, potentially leading to post-operative brain edema.[25,26] Collateral vessels develop through a process known as angiogenesis (the formation of collateral arteries and veins) may serve as a compensatory mechanism as a primary blood vessel gradually becomes obstructed. However, Florisson *et al.* proposed that collateral branches may reflect congenital abnormalities of the venous system rather than compensation mechanisms for increased intracranial pressure.[27] Therefore, evaluating venous sinus collateral circulation is important for supporting spontaneous and therapeutic thrombosis, and accurately identifying side branches could provide further information for the functional compensation of venous sinus stenosis.[28,29] In the present study, MRI-based evaluation allowed for the observation of more detailed collateral vessels, suggesting the potential for enhanced understanding of the functional significance of anatomic abnormalities in the TS and SS.

4.3. Clinical application

Computational fluid dynamics (CFD) simulation has emerged as a valuable tool for studying idiopathic intracranial hypertension.[30,31] The accuracy of patient-specific CFD simulations of hemodynamics depends significantly on the geometries. In the present work, we observed variations between CTV- and MRI-based 3D geometric reconstructions that could significantly impact simulations. As a result, hemodynamic analyses may vary, potentially leading to misinterpretation of sinus drainage in transient flow simulations. Our results of geometric reconstructions indicated a high degree of similarity between the geometries derived from CTV and MRI. While the distributions of stenosis exhibited high consistency between CTV and MRI, notable variations were observed in anatomical parameters. Although advanced MRI can visualize intracranial venous hemodynamics in patients with and without PT,[32] a more comprehensive understanding of hemodynamics is not solely attainable through MRI assessment, as invasive examinations remain the gold standard for measuring trans-stenotic pressure. Further, evaluation of the impact of geometries on hemodynamics is necessary to determine the optimal choice of imaging modalities for subsequent CFD simulations.

4.4. Limitations

Several limitations were identified in this study. First, the sample size was small, potentially compromising statistical power. Our analysis primarily focused on patients with PT to evaluate additional anatomical variations related to stenosis. While this approach may introduce clinical bias, our results

underscored the potential impact of non-invasive imaging modalities on anatomical analysis. Further investigation is warranted to justify the prevalence of such variations to facilitate the more convenient diagnosis of venous abnormalities related to PT. Second, digital subtraction angiography (DSA) was not incorporated in this study. Despite its utility in detecting vascular abnormalities in PT patients, the invasiveness of DSA has restricted its use exclusively to guide interventional radiology procedures.[33] However, DSA has demonstrated superior performance in assessing collateral venous drainage. Hence, further evaluation is required to evaluate the impact of additional drainage on comprehensively understanding PT diagnosis.[32] Thirdly, CTV data and visual-based vein segmentation served as the reference in the present study. To mitigate human error, geometric reconstruction was conducted with input from experts. In addition, repeated measurements were conducted to assess the consistency of visual-based evaluations, revealing a high correlation between measurements.

5. Conclusion

MRI has demonstrated high efficacy in assessing venous sinus stenosis when compared to CTV as a reference. In addition, MRI offers enhanced visualization of collateral vessels, thereby potentially facilitating a more accurate diagnosis of the functional significance of venous sinus stenosis based on anatomical analysis. While CTV-based evaluations may be affected by the bone structures surrounding the venous sinus, MRI-based evaluations primarily focus on blood flow within the segments, thus enabling the detection of both anatomical and functional abnormalities.

Acknowledgments

None.

Conflict of interest

The authors declare that they have no competing interests.

Author contributions

Conceptualization: Xin Liu, Heyu Ding, Zhenchang Wang
Formal analysis: Pengfei Zhao, Shusheng Gong
Investigation: Xin Liu, Zhenxin Hong, Heyu Ding
Methodology: Xin Liu, Zhenxin Hong, Heyu Ding
Writing – original draft: Xin Liu, Zhenxin Hong
Writing – review & editing: Xin Liu, Dhanjoo Ghista

Ethics approval and consent to participate

The Research Ethics Committee of Beijing Friendship Hospital, Capital Medical University, approved this study (Ethics approval code: 2023-P2-095-01). Data were collected retrospectively, and no further procedure was performed; hence, informed consent was waived.

Consent for publication

All images used in this study were anonymized; hence, consent for publication was waived.

Availability of data

The data used in this study will be made available on request after publication.

References

1. Essibayi MA, Oushy SH, Lanzino G, Brinjikji W. Venous causes of pulsatile tinnitus: Clinical presentation, clinical and radiographic evaluation, pathogenesis, and endovascular treatments: A literature review. *Neurosurgery*. 2021;89(5):760-768.

    doi: 10.1093/neuros/nyab299

2. Nicholson P, Brinjikji W, Radovanovic I, *et al*. Venous sinus stenting for idiopathic intracranial hypertension: A systematic review and meta-analysis. *J Neurointerv Surg*. 2019;11(4):380-385.

    doi: 10.1136/neurintsurg-2018-014172

3. Zhao P, Ding H, Lv H, *et al*. CT venography correlate of transverse sinus stenosis and venous transstenotic pressure gradient in unilateral pulsatile tinnitus patients with sigmoid sinus wall anomalies. *Eur Radiol*. 2021;31(5):2896-2902.

    doi: 10.1007/s00330-020-07415-2

4. Zhao P, Lv H, Dong C, Niu Y, Xian J, Wang Z. CT evaluation of sigmoid plate dehiscence causing pulsatile tinnitus. *Eur Radiol*. 2016;26:9-14.

    doi: 10.1007/s00330-015-3827-8

5. Li Y, Chen H, He L, *et al*. Hemodynamic assessments of venous pulsatile tinnitus using 4D-flow MRI. *Neurology*. 2018;91(6):e586-e593.

    doi: 10.1212/WNL.0000000000005948

6. Heyu D, Pengfei Z, Han L, *et al*. A new method for assessing transverse sinus stenosis with CT venography based on the venous trans-stenotic pressure gradient. *J Neurointerv Surg*. 2023;15(10):1034-1038.

    doi: 10.1136/jnis-2022-019270

7. Patel D, Machnowska M, Symons S, *et al*. Diagnostic performance of routine brain MRI sequences for dural venous sinus thrombosis. *AJNR Am J Neuroradiol*. 2016;37(11):2026-2032.

doi: 10.3174/ajnr.A4843

8. Ghoneim A, Straiton J, Pollard C, Macdonald K, Jampana R. Imaging of cerebral venous thrombosis. *Clin Radiol*. 2020;75(4):254-264.

doi: 10.1016/j.crad.2019.12.009

9. Dmytriw AA, Song JS, Yu E, Poon CS. Cerebral venous thrombosis: State of the art diagnosis and management. *Neuroradiology*. 2018;60:669-685.

doi: 10.1007/s00234-018-2032-2

10. Provenzale JM, Kranz PG. Dural sinus thrombosis: Sources of error in image interpretation. *Am J Roentgenol*. 2011;196(1):23-31.

doi: 10.2214/AJR.10.5323

11. Lansley JA, Tucker W, Eriksen MR, Riordan-Eva P, Connor SE. Sigmoid sinus diverticulum, dehiscence, and venous sinus stenosis: Potential causes of pulsatile tinnitus in patients with idiopathic intracranial hypertension? *Am J Neuroradiol*. 2017;38(9):1783-1788.

doi: 10.3174/ajnr.A5277

12. Sarma A, Martin D, Pruthi S, Jones R, Little SB. Imaging the cerebral veins in pediatric patients: Beyond dural venous sinus thrombosis. *Radiographics*. 2023;43(2):e220129.

doi: 10.1148/rg.220129

13. Pallewatte AS, Tharmalingam T, Liyanage N. Anatomic variants and artefacts in non enhanced MRV-Potential pitfalls in diagnosing cerebral venous sinus thrombosis (CVST). *Sri Lanka J Radiol*. 2016;2(1):40.

doi: 10.4038/sljr.v2i1.23

14. Kobayashi K, Matsui O, Suzuki M, Ueda F. Anatomical study of the confluence of the sinuses with contrast-enhanced magnetic resonance venography. *Neuroradiology*. 2006;48:307-311.

doi: 10.1007/s00234-006-0065-4

15. Buyck PJ, Zuurbier SM, Garcia-Esperon C, *et al*. Diagnostic accuracy of noncontrast CT imaging markers in cerebral venous thrombosis. *Neurology*. 2019;92(8):e841-e851.

doi: 10.1212/WNL.0000000000006959

16. Vymazal J, Rulseh AM, Keller J, Janouskova L. Comparison of CT and MR imaging in ischemic stroke. *Insights Imaging*. 2012;3:619-627.

doi: 10.1007/s13244-012-0185-9

17. Guryildirim M, Kontzialis M, Ozen M, Kocak M. Acute headache in the emergency setting. *Radiographics*. 2019;39(6):1739-1759.

doi: 10.1148/rg.2019190017

18. Pereira VM, Cancelliere NM, Najafi M, *et al*. Torrents of torment: Turbulence as a mechanism of pulsatile tinnitus secondary to venous stenosis revealed by high-fidelity computational fluid dynamics. *J Neurointerv Surg*. 2021;13(8):732-737.

doi: 10.1136/neurintsurg-2020-016636

19. Gao L, Xu W, Li T, *et al*. Accuracy of magnetic resonance venography in diagnosing cerebral venous sinus thrombosis. *Thromb Res*. 2018;167:64-73.

doi: 10.1016/j.thromres.2018.05.012

20. Ruíz DS, Gailloud P, Rüfenacht DA, Delavelle J, Henry F, Fasel JH. The craniocervical venous system in relation to cerebral venous drainage. *Am J Neuroradiol*. 2002;23(9):1500-1508.

21. Boddu S, Dinkin M, Suurna M, Hannsgen K, Bui X, Patsalides A. Resolution of pulsatile tinnitus after venous sinus stenting in patients with idiopathic intracranial hypertension. *PLoS One*. 2016;11(10):e0164466.

doi: 10.1371/journal.pone.0164466

22. Farrag A, Irfan M, Guliani GK, *et al*. Occurrence of post-acute recanalization and collateral formation in patients with cerebral venous and sinus thrombosis. A serial venographic study. *Neurocrit Care*. 2010;13:373-379.

doi: 10.1007/s12028-010-9394-6

23. Mazur MD, Cutler A, Couldwell WT, Taussky P. Management of meningiomas involving the transverse or sigmoid sinus. *Neurosurg Focus*. 2013;35(6):E9.

doi: 10.3171/2013.8.FOCUS13340

24. Sheth SA, Trieu H, Liebeskind DS, *et al*. Venous collateral drainage patterns predict clinical worsening in dural venous sinus thrombosis. *J Neurointervent Surg*. 2018;10(2):171-175.

doi: 10.1136/neurintsurg-2016-012941

25. Tanaka M, Imhof HG, Schucknecht B, Kollias S, Yonekawa Y, Valavanis A. Correlation between the efferent venous drainage of the tumor and peritumoral edema in intracranial meningiomas: Superselective angiographic analysis of 25 cases. *J Neurosurg*. 2006;104(3):382-388.

doi: 10.3171/jns.2006.104.3.382

26. Inamura T, Nishio S, Takeshita I, Fujiwara S, Fukui M. Peritumoral brain edema in meningiomas--influence of vascular supply on its development. *Neurosurgery*. 1992;31(2):179-185.

doi: 10.1227/00006123-199208000-00002

27. Florisson JM, Barmpalios G, Lequin M, *et al*. Venous hypertension in syndromic and complex craniosynostosis: The abnormal anatomy of the jugular foramen and collaterals. *J Craniomaxillofac Surg*. 2015;43(3):312-318.

28. Huang YC, Lee JD, Pan YT, Weng HH, Yang JT, Lin LC. Perfusion defects and collateral flow patterns in acute small subcortical infarction: A 4D dynamic MRI study. *Transl Stroke Res*. 2022;13:339-409.

doi: 10.1007/s12975-021-00953-x

29. Venema SM, Dankbaar JW, Wolff L, *et al.* Collateral status and recanalization after endovascular treatment for acute ischemic stroke. *J Neurointerv Surg.* 2023;15(6):531-538.

    doi: 10.1136/neurintsurg-2021-018545

30. Hatami H, Danesh N, Shojaei M, Hamedani AR. Evaluation of diagnostic values in NCCT and MRI of the patients with cerebral venous or sinus thrombosis in loghman hakim Hospital in Tehran 2014-2018. *Int Clin Neurosc J.* 2019;6(1):17-21.

31. Stoumpos S, Tan A, Hall Barrientos P, *et al.* Ferumoxytol MR angiography versus duplex US for vascular mapping before arteriovenous fistula surgery for hemodialysis. *Radiology.*

2020;297(1):214-222.

    doi: 10.1148/radiol.2020200069

32. Bonatti M, Valletta R, Lombardo F, *et al.* Accuracy of unenhanced CT in the diagnosis of cerebral venous sinus thrombosis. *Radiol Med.* 2021;126:399-404.

    doi: 10.1007/s11547-020-01263-2

33. Qiu X, Zhao P, Li X, *et al.* The relationships among transverse sinus stenosis measured by CT venography, venous trans-stenotic pressure gradient and intracranial pressure in patients with unilateral venous pulsatile tinnitus. *Front Neurosci.* 2021;15:694731.

    doi: 10.3389/fnins.2021.694731

Appendix
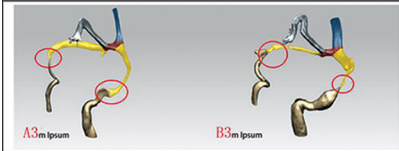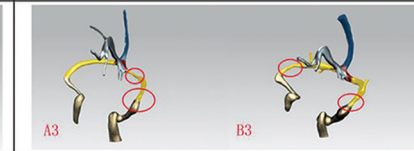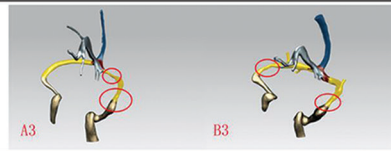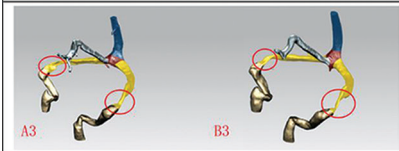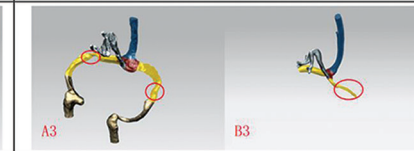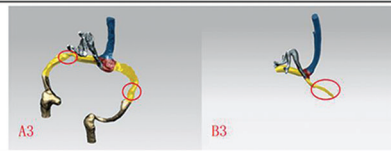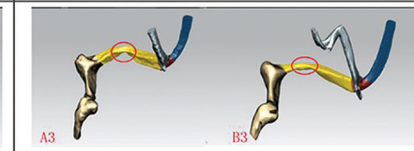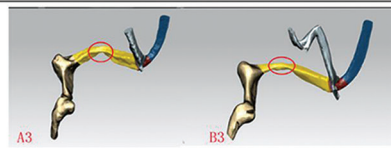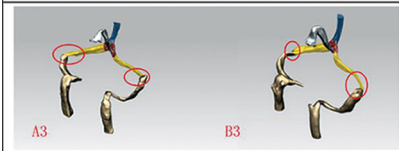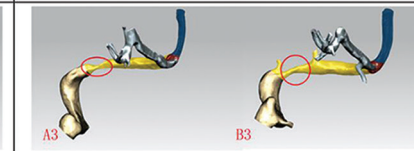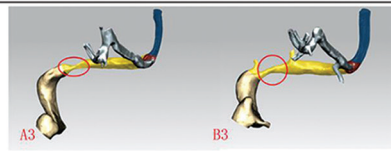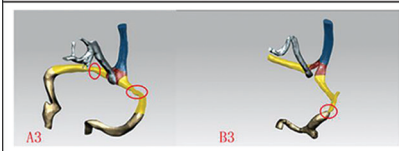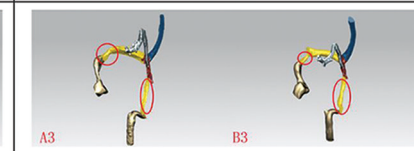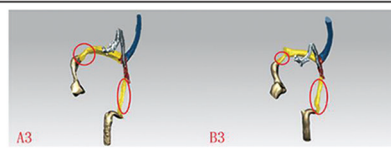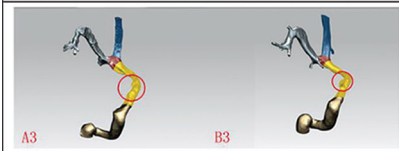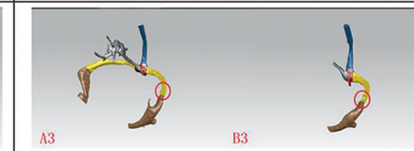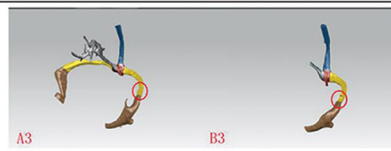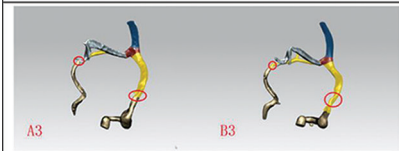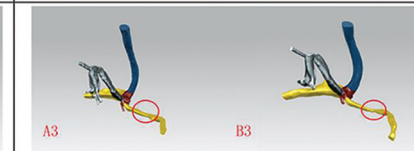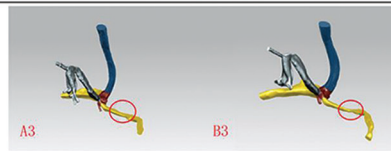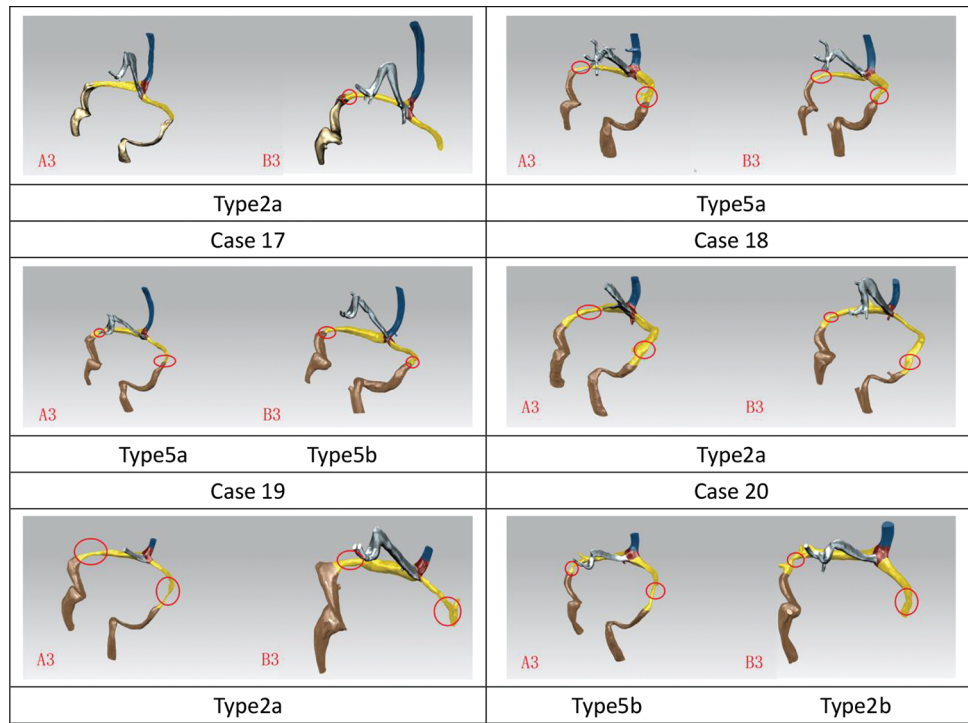

Figure A1. *(Cont'd...).*

(Continued)

Figure A1. Sinus-wise analysis to compare the number of inlets and outlets between computed tomography (CT)-and magnetic resonance imaging (MRI)-based geometric reconstructions. In general, more inlets were observed at the superior sagittal sinus in CT-based geometric reconstructions, with the exception of Cases 7, 10, 15, 16, 18, and 19. Conversely, additional outlets were detected at the sigmoid sinus (SS) in MRI-based reconstructions for Cases 1, 5, 7, 8, 9, 10, 13, 15, 16, 17, 18, and 19.
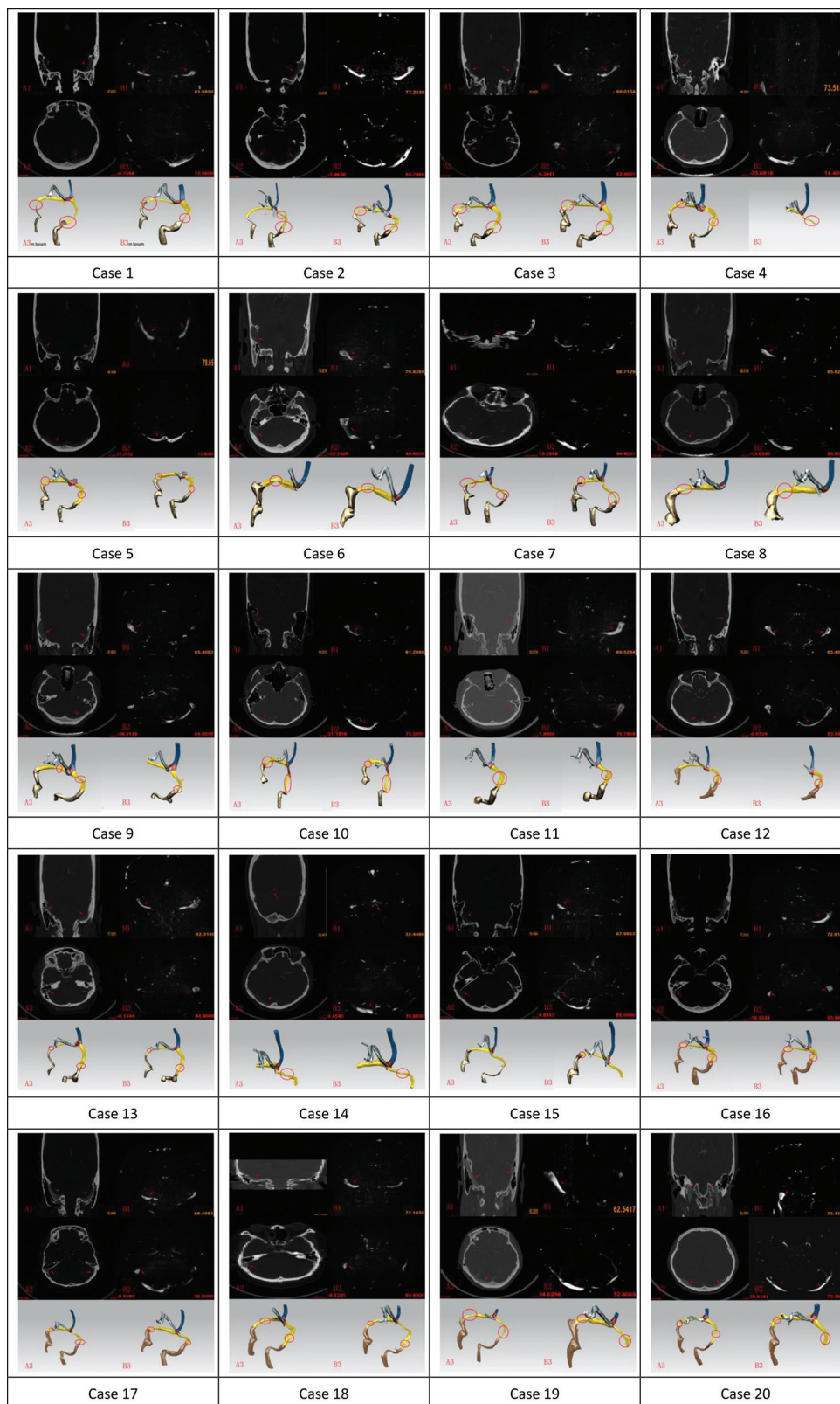
Figure A2. The case analysis in the present study. For each case, the left column illustrates the computed tomography-based results, while the right column presents the magnetic resonance imaging-based analysis. The first row displays the coronary plane relative to the transverse sinus. The second row depicts the transverse plane relative to the beginning of the sigmoid sinus. The third row showcases the three-dimensional geometric reconstructions based on the images.